Application of AAO Matrix in aligned gold nanorod array substrates for surface enhanced fluorescence and Raman scattering

Signe Damm [†], Frances Lordan [†], Antony Murphy [‡], Mark McMillen [‡], Robert Pollard [‡], James H. Rice *[,†]

[†] NanoPhotonics Research Group, University College Dublin, Belfield, Dublin 4, Ireland.
[‡] Department of Physics and Astronomy, Queen's University Belfast, University Road, Belfast BT7 1NN, UK.
* Corresponding author. E-mail: james.rice@ucd.ie

Keywords: SERS, SEF, Au Nanorod, Alumina template, NaOH etching, Rhodamine 6G

Abstract

In this paper we probe surface enhanced Raman scattering (SERS) and Surface enhanced Fluorescence (SEF) from probe molecule Rhodamine 6G (Rhod6G) on self-standing Au nanorod array substrates made using a combination of anodization and potentiostatic electro-deposition. The finished substrates were embedded within a porous alumina template. By varying the etching time i.e. the thickness of the alumina, we show that there exists an inverse relationship between SERS and SEF. SERS and SEF also show a nonlinear response to increasing etching time due to an inhomogeneous plasmon activity across the nanorod. By modeling the electromagnetic fields created at different etching times we confirm the nonuniform plasmon activity along the Au nanorods and explain the nonlinear behaviors of SERS and SEF. Optimization of the level of alumina matrix thickness optimizes conditions for obtaining either maximized SERS, SEF or for simultaneously observing both SERS and SEF together.

Introduction

Nanoscale structures made from metals such as gold or silver possess localized surface plasmon (LSP) excitations when the material interacts with light of the correct frequency and polarization.[1-8] When LSPs are formed, strongly enhanced electromagnetic near-fields are generated at the surface of the supporting nanostructure. This property has attracted considerable research interest due to its potential applications in sensors, photonic circuits and medical diagnostics and therapeutics. Modern nanofabrication methodologies enable the creation of a number of different nanostructures with precisely controlled shapes, sizes, and spacings.[9-14] One particular area of active research within plasmonics is the investigation of the effect of nanostructure substrate geometry on the optical properties of materials in the near-field of the LSP.[4,5,7,8,15]

Nanostructured metal dielectric interfaces in nanoscale thick metal films can couple light with LSP to produce a reflectance spectrum that is sensitive to changes in surface dielectrics.[7,8,15] The interaction of metal nanoparticles and roughened nanostructured films with light can create localized surface plasmon resonances (LSPRs). Such LSPRs possess wavelength-selective extinction sensitive to surface dielectric, composition, particle size and

shape. Periodic metal nanoparticle arrays have been shown to produce LSPRs.[7,8,15] The LSPRs are influenced by modulating changes in diameter or spacing ratios between the nanoparticles. Metallic nanostructures that possess anisotropic symmetry, such as nanorods, are reported to produce LSPRs with high quality factors.[16-19] Nanorod array design enables choice over precise particle shape, length, width and inter-particle coupling. Such nanorod arrays have been reported to support negative refraction at visible to near-infrared wavelengths or provide near-field focusing for sub-wavelength imaging.[18,19]

Lyvers et al. demonstrated that two-dimensional (2D) hexagonal arrays of Au nanorods, prepared by galvanostatic electro-deposition, support plasmon resonance modes at both visible and near-infrared wavelengths when coupled with light at normal incidence.[20] The authors demonstrated that the nanorod arrays possessed multiple resonant attenuations, the properties of which were controlled by the nanorod height and the dielectric medium. The nanorods were reported to possess harmonic sets of longitudinal standing waves in cavities between nanorods with nodes and antinodes of the plasmon modes bound at the base and tips of the array. Notably the number of harmonic resonances and their frequencies could be adjusted as a function of nanorod height, diameter-spacing ratio and the refractive index of the host medium. Pollard et al. demonstrated that the optical properties of 2D nanoarray of nanorods, grown by direct electrodeposition, possessed properties associated with epsilon-near zero metamaterials in which components of the real part of dielectric permittivity approaches zero.[18,19] 2D nanorod arrays have been applied to enable surface-enhanced Raman scattering (SERS) spectra from molecules adsorbed on the surface of vertically aligned gold nanorod arrays In addition, gold nanorods possess good chemical stability and biocompatibility under biological conditions. [17,21]

Fluorescence spectroscopy is another well-known spectroscopic method playing a major role in selective detection of bioanalytes.[23] Similarly to the effect of increasing the Raman scattering of molecules, the presence of LSPRs on plasmonic metal nanostructures can enhance the fluorescence signal from locally situated fluorophores, a process known as metal enhanced (MEF) or surface enhanced fluorescence (SEF).[23] SEF occurs when the fluorophore is within an optimum range of distances from the metal. This process creates a more efficient emitter, eliminates metal induced quenching, reduces photobleaching rate and increases photostability of fluorophores. Few reports have studied SERS and SEF together which is potentially attractive for sensor applications.[3,7] One challenge to this approach is to fabricate conditions that enable both SERS and SEF responsive from nanoprobes as the optimum distance for enhancing fluorescence emission and Raman scattering is different.

In this paper we simultaneously study the conditions for maximizing SERS and SEF from Au nanorods, by utilizing the alumina matrix surrounding the nanorods after fabrication. Studies on SERS active sites have shown that rod tips are the main contributors to the enhancement and as a result the SERS response has shown to be non-linear with etching time. [24-26] Controlled aggregation of rod tips has shown to cause high SERS intensities when the analyte is able to adsorb in between the aggregated tips.[25] Collapse of nanorods prior to adsorption of the analyte have shown to decrease the SERS intensity. [24-26] This is due to increased difficulty for the analyte to adsorb onto areas of "hot spots" [25] and loss of integrity of the 2D array. [24,27] Previous studies have shown that long range order of the 2D nanorod array has a great impact on both local and long range enhancement of the EM-field.[27] Studies on the SEF response in the presence of different amounts of alumina are yet to be explored. Using alumina as a dielectric spacer we study the thickness of alumina for optimization of SEF and simultaneously locate the SERS active sites on the nanorods. We show that there exists an

inverse relationship between SERS and SEF. To support the experimental findings we carry out 3D FEM calculations.

Experimental setup

A schematic illustration of the sample i.e. a quasi-ordered free-standing Au nanorod array substrates, is shown in Fig. 1a along with a SEM image (using a Jeol 6500F field emission SEM) shown as inset. SEM data showed that the arrays possessed average spacing (center-to-center) 70 nm, rod diameter 35 nm and rod height of 200 nm. A pre-cleaned glass substrate was used as a base for the nanorod fabrication (SCHOTT UK Limited). On this a thin film multilayer was prepared by magnetron sputtering, consisting of 8 nm tantalum pentoxide (Ta_2O_5), 5 nm gold and a 400 nm aluminium film. Porous alumina (PAO) templates were formed by anodization of the aluminium in 0.3 M sulphuric acid (~1°C) at constant voltage (40V) using a platinum counter-electrode. Au nanorods were then grown in the PAO template by electrodeposition from the conducting 5 nm thick Au under-layer. The samples were annealed at 200 °C for 2h before 0.1 M NaOH was used to etch the alumina matrix according to the following reaction:

$$Al_2O_3 + 2NaOH \rightarrow 2NaAlO_2 + H_2O \qquad (1)$$

The SERS response of the substrates was investigated by using probe molecule Rhodamine 6G (Rhod6G) which possess Raman scattering as well as fluorescence with 532 nm excitation.[7,8] The substrates were immersed in 0.1mM aqueous solution of Rhod6G for 24 hours, rinsed in distilled water and allowed to dry, leaving a layer of adsorbed probe molecules on the gold surface. Raman and fluorescence spectra were recorded using a custom-built, open-bench system in epi-fluorescence backscattering configuration with a 50x objective and 532 nm excitation at a power of 0.5mW.[7,8] The degree of removal of alumina was seen to affect SEF and SERS efficiency differently. A study of etching time vs. SERS and SEF was performed using a number of identical substrates, each one given a different etching time before the probe molecule was applied.

Results

Fig. 1b shows the absorption and emission spectra from Rhod6G together with the normal incidence absorption spectrum for the Au nanorod substrate before etching. The absorption spectrum of the Au nanorod substrate shows a strong transverse mode at c.a. 530 nm (T) and a mode at c.a. 670 nm, originating from the Au underlayer (U). As shown, Rhod6G emission and absorption band overlaps with the plasmon resonance of the Au nanorod substrate.

Directly after growth, the gold nanorod array is surrounded by an alumina matrix which initially stands 100 nm taller than the Au nanorods. Fig. 2a-f show schematics of the alumina surrounding the Au nanorods for etching times 0 (a-i), 2.5 (b-i) and 7.5 min (c-i). The figure also shows SEM images of the alumina matrix being selectively removed using six different etching times 0 (a-ii), 2.5 (b-ii) 7.5 (c-ii) 20 (d) 35 (e) and 40 min (f). As seen in Fig. 2a-f, there are two facets to the sodium hydroxide etch; firstly it reduces the height of the alumina matrix, and secondly, widens the pore, creating a shell space around the central nanorod. As the etching time is increased, more probe molecules are able to adsorb onto the exposed surface of the Au nanorods.

To study the morphology and quality of the samples after each etching step we preform UV-VIS spectroscopy. In fig. 1b, the normal incidence absorption spectrum for the nanorod substrate before etching shows a strong transverse mode at c.a. 530 nm (T) and an underlayer mode at c.a. 670 nm, originating from the Au underlayer (U). Fig. 2g shows the normal incidence UV-visible absorption spectra for a series of identical Au nanorod substrates with different etching times. As etching time is increased the T mode decreases in overall intensity while the U mode increases. This change is due to two things; strengthening of the plamonic coupling between the Au underlayer and the Au nanorod and change in dielectric sorounding the nanorods as the alumina is etched away. The longitudinal mode (L) of the nanorods is excited by tilting the sample, so the incident field has a component in the direction of the long axis of the rod. Absorption spectra at 40 degree angle of incidence show an increasing L mode relative to the spectra recorded at normal incidence (see inset in Fig. 2g). This indicates that the nanorods are initially in the predominantly perpendicular direction as shown in the SEM images in Fig. 2a-c. The resonance of the L mode is dependent on dielectric medium, i.e. a blue shift is measured with decreasing alumina, from 640nm (2.5min) to 560 nm (35min). At high etch time (>35 min) the plasmonic modes become less distinctive in the absorption spectrum. This suggests that releasing the nanorods from the alumina matrix causes the nanorods to start bending, with the long axis of the nanorods having a component parallel to the substrate. As the etching time is further increased (>40min), the nanorods start collapsing and no distinct modes are observed. The corresponding SEM images of the nanorods are shown in Fig. 2d-f.

The effect of etching time on the SEF and SERS spectral intensities was studied. Fig. 2h shows SEF spectra recorded for different etching times along with SERS spectra recorded simultaneously from the same substrate (inset). For comparison the SEF recorded using a glass substrate is also shown. With a short etch time e.g. 2.5 min the intensity of SEF shows a 2 fold enhancement compared to the emission intensity recorded using glass, thereafter, with increasing etching time, SEF intensity is reduced. Conversely, as etching time increases, the SERS signal increases. Fig. 3a shows a plot of SEF (■) and SERS (●) signal intensities as a function of etching time. SERS intensity increases rapidly with increasing etching time until it saturates after approximately 25 min of etching. As seen in Fig. 3a, we measure SERS to initially be proportional to etching time as more gold become available. But after 10 min. etching, we measure a more modest increase in SERS with increasing etching time. The nonlinear SERS response indicates an inhomogeneous distribution of SERS active sites, with rod tips being dominant. It is possible hot spots are present along the side of the nanorods due to roughness created upon fabrication. Nevertheless the experimental data indicate that the tips of the rods are the dominant contributors to SERS. After approx. 25 min of etching, the SERS intensity saturates, due to the Au nanorods being fully exposed and all alumina etched away. Further etching results in lower reproducibility in SERS caused by bending and in the end collapse of the Au nanorods (data not shown). The collapse occasionally creates areas of high SERS intensity due to “hot spots”. But mainly we observe a decrease in SERS intensity originating from loss of periodicity and integrity of the 2D array.

Fig. 3a shows a rapid increase in SEF intensity between etching times of 0 and 2.5 min. The occurrence of high SEF from the nanorods following etching for a short period of time is assigned to arise from a high plasmon activity around the Au nanorod combined with the probe molecule being at an optimum distance. Additional etching time results in a rapid decrease in SEF, as more gold and less alumina become available, until the intensity settles.
Fig. 3b shows the resulting optimized fluorescence and Raman signals from Rhod6G on a Au nanorod substrate. To obtain maximum fluorescence and Raman signals, the samples were

etched for 2.5 min and 35 min respectively. Studies concentrating on the Raman spectrum alone showed that no signal could be seen from glass with the same concentration of probe molecule, while a relatively strong and clear Raman spectrum was recorded using the nanorod substrate. This supports the assertion that the Raman spectra recorded are SERS. Studies on fluorescence showed a 2-fold enhancement compared to glass, confirming SEF.
Fig. 3c shows a plot of SEF vs. SERS intensity. A rapid decrease in SEF results in an equal rise in SERS intensity i.e. a linear relationship is shown. The plot shows that at etching times resulting in highest SEF intensity, we observe the lowest SERS intensity and vice versa. As SERS reaches $1.5 \cdot 10^4$ in intensity the SEF intensity reaches minimum as quenching of the SEF is fully activated.

The reproducibility of the SERS and SEF signal on the substrate was examined. Studying the SERS spectral features recorded over different areas of the sample show that the degree of change was <5% in regard to signal intensity. The change in SEF signal intensity levels over the substrate was also studied. The degree of change in SEF was measured to be <15%. SERS is less sensitive to the presence of aggregates than SEF, as SERS arises only from where the probe molecule is directly in contact with the metal. In comparison surface plasmons enhance the fluorescence to a much lesser extent. The variation in SEF intensity is assigned to arise from aggregation of the probe molecule creation small areas of strong luminescence from the sample e.g. dye aggregates.

FEM calculations
Finite element methods is used to calculate the electric fields around the gold nanorod for various etching time of the surrounding matrix, from which the authors suggest an explanation for the behavior of SEF. There is here a clear physical problem. Electric field enhancement cannot explain SEF by itself: one should at least compare radiative and non radiative electromagnetic modes. Indeed, the results presented in the manuscript clearly show that SEF is higher near glass substrates rather than in the proximity of metal surface. In comparison, the analysis of SERS results is almost inexistent.m

To further investigate the behavior of SERS and SEF with etching time, 3D calculations of the electromagnetic near fields on the Au nanorod substrate were carried out using RF module within COMSOL multiphysics (finite element analysis). A model was made using a single nanorod with dimensions determined by SEM images (see Fig. 2a-f). The Au nanorod was embedded in a varying combination of air (n_{air}=1) and alumina (n_{alu}=1.78). The dielectric constant of gold was taken from Johnson and Christy.[29] The thickness and height of the alumina was made according to SEM images at different etching times and to create a nanorod array, periodic boundary conditions were applied. The nanorod was excited at normal incidence for a range of wavelengths between 400-900nm. The etching process was assumed symmetrical and therefore independent on the incident polarization of the E-field in the plane perpendicular to the long axis of the rod (xy plane). At this configuration only the transverse, and not the longitudinal mode, was excited.

Fig. 4a-e shows the results of the calculations and makes comparisons with experimental results. Fig. 4a shows images of the E-field distribution around the nanorod for different etching times. The E-field intensity is color coded according to the color bar. It is evident from the images that there exists a non-uniform distribution of the E-field along the rod, with the edges at the tip accumulating the highest E-fields. Noticeable is also that at low etch times highly localized E-fields are created between the alumina and Au nanorod. Fig. 4b shows the result of measuring the E-field for different excitation wavelength for the substrate etched for

7.5min (2). The result is compared with experimental measured absorption of the Au nanorod substrate after 7.5 min etching (1). There exists a good correlation between the two, indicating the enhancing field from the nanorod is in fact originating from the excitation of the transverse mode absorbing at 530 nm.

The schematic in Fig. 4c shows the area on the Au nanorod surface used for calculating the spatial average E-field (E_{avg}). It is well known that Raman enhancement is proportional to the E-field to the power of 4 [30], so therefore E_{avg}^4 has been calculated and compared with SERS intensity. The calculated E_{avg}^4 (▲) is plotted against etching time in Fig. 4d along with the SERS (●) and SEF (■) intensities. The intensities have been normalized to clearly show the degree of change with etching time. At low etch times (~2min) we calculate the highest E-field intensity, due to the narrow gap of 5 nm created between the alumina and Au nanorod. As the alumina is etched away the E-field decrease and is almost unchanged after approx. 5 min of etching corresponding to a 12.5 nm gap between alumina and Au nanorod. When comparing the calculated E-field with experimental SERS intensity it shows little correlation between the two. It is possible the SERS is unaffected by the intense E-field a low etch times because of the narrow gap between the Au and alumina, restricting access to the probe molecule. Long Au nanorods have been shown to be hydrophobic. [31] Even though our nanorods are relatively short, with much of the alumina still present it can be difficult to properly wet the Au nanorods with the probe solution. Since the calculated E-field is almost unchanged after 5 min. of etching we conclude that the increase in SERS with etching time is due to an increase in Au surface area available to the probe molecule. The ratio of alumina to Au surface area decreases with increasing etching time, causing an increase of SERS until the alumina is fully etched away and the SERS intensity saturates. When the Au nanorods are fully exposed they are sensitive to breakage. This can be an advantage or a disadvantage. Bending of the nanorods towards each other can create “hot spots”, increasing SERS intensity. But a complete collapse of the nanorods destroys the integrity of the array, causing a decrease in SERS intensity. As a result, we observe SERS intensities of higher variation beyond 25 min etching.

The behavior of SEF intensity at low etch time indicates that the probe molecule adsorbed onto the alumina is affected by the strong E-field created in the narrow gap between Au and alumina. Fig. 4e shows a diagram of probe molecules adsorbed onto the alumina and Au surface. This diagram corresponds to a low etch time (~1-2min), where the probe molecule is predominantly adsorbed onto the alumina but still affected by the high E-field generated between the alumina and the Au nanorod . This creates a good platform for producing SEF. As the ratio of alumina to Au surface area decreases, the probe molecule is able to adsorb onto the Au nanorod and the fluorescence is effectively quenched corresponding to a decrease in SEF intensity. This method makes it possible to tune the samples to maximize either SERS or SEF depending on application. By etching the alumina for 5 min simultaneous SERS and SEF signals can be obtained. It is noted that electric field enhancement cannot alone explain SEF, consideration of such factors as radiative and non-radiative electromagnetic modes is required.

Conclusion

In conclusion, we have shown that the effect of etching time is different for SEF and SERS. SEF intensity initially increases as the substrate is etched for ~1-2 min. This increase is believed to be due to a combination of high E-field generated around the Au nanorod and the optimum distance between probe molecules and Au surface. After an initial increase, the SEF

intensity decreases with increasing etching time as quenching of the fluorescence becomes dominant. This is caused by the increased number of probe molecules in direct contact with the Au nanorods. In contrast, SERS intensity increases with increasing etching time as more of the Au nanorod is exposed and available to the probe molecule. We have shown that there exist an inverse relationship between SERS and SEF and that it is possible to tune and optimize SERS and SEF. COMSOL calculations confirm the non-uniform E-field distribution on the surface of the Au nanorod and also the nonlinearity in SERS and SEF intensities with etching time. By utilizing the alumina template we demonstrate a simple way to control the enhancement of Raman and fluorescence signals without adding any additional elements to the substrates.

Acknowledgement

This work was supported by grants from Science Foundation Ireland (SFI P.I. 09/IN.1/B2650) and (10/IN.1/B3025). The Nanophotonics and Nanoscopy Research Group is supported by SFI grants 11/RFP.1/MTR/3151, 12/IP/1556 and 09/RFP/PHY2398. A. Murphy, M. McMillen and R. J. Pollard would like to acknowledge support from EPSRC.

References

1. S. Hayashi and T. Okamoto, *J. Phys. D: Appl. Phys.*, 2012, **45** (43), 433001.
2. N. Al-Alttar, I. Kopf, K. Flavin, E. Kennedy, S. Giordani and J. H. Rice, *Chem. Phys. Lett.*, 2013, **568–569**, 95–100.
3. F. Lordan S. Damm, N. Al-Attar, C. Mallon, R. J. Forster, T. E. Keyes and J. H. Rice, *Plasmonics*, 2012, DOI 10.1007/s11468-013-9573-3
4. S. Damm, N. C. Carville, B. J. Rodriguez, M. Manzo, K. Gallo and J. H. Rice, *J. Phys. Chem. C.*, 2012, **116**, 26543–26550.
5. N. C. Carville, M. Manzo, S. Damm, M. Castiella, L. Collins, D. Denning, S. A. L. Weber, K. Gallo, J. H. Rice and B. J. Rodriguez, *ACS Nano*, 2012, **6**, 7373–7380.
6. N. Al-Alttar, E. Kennedy, I. Kopf, S. Giordani and J. H. Rice, *Chem. Phys. Lett.*, 2012, **535**, 146-151.
7. F. Lordan, J. H. Rice, B. Jose, R. J. Forster and T. E. Keyes, *J. Phys. Chem. C*, 2012, **116**,1784.
8. F. Lordan, J. H. Rice, B. Jose, R. J. Forster and T. E. Keyes, *Appl. Phys. Lett.*, 2011, **99**, 033104.
9. R. A. Taylor, J. W. Robinson, J. H. Rice, J. D. Smith, R. A. Oliver, G. A. D. Briggs, M. J. Kappers, C. J. Humphreys and Y. Arakawa, *Physica E*, 2003, **21**, 285-288.
10. J. H. Rice, R. Aures, J. P. Galaup and S. Leach, *Chemical Physics*, 2001, **263**, 401-414.
11. J. H. Ne, Y. S. Park, J. H. Rice and R. A. Taylor, *Applied Physics Letters*, 2005, **86**, 083109-083112.
12. R. W. Martin, P. R. Edwards, R. A. Taylor, J. H. Rice, J. H. Na, J. W. Robinson, J. D. Smith, C. Liu and I. M. Watson, *Physica Status Solidi A*, 2005, **202**, 372-374.
13. J. H. Rice, J. P. Galaup and S. Leach, *Chemical Physics*, 2002, **279**, 23-41.
14. J. H. Rice, R. A. Oliver, G. A. D. Briggs, M. J. Kappers, C. J. Humphreys, J. D. Smith and R. A. Taylor, *Physica E*, 2004, **21**, 546-548.
15. X. V. Li, R. M. Cole, C. A. Milhano, P. N. Bartlett, J. J. Baumberg, B. F. Soares and C. H. De Groot, *Nanotechnology*, 2009, **20** (28), 285309-285316.
16. A. Murphy, Y. Sonnefraud, A. V. Krasavin, P. Ginzburg, F. Morgan, J. McPhillips, G. Wurtz, S. A. Maier, A. V. Zayats and R. Pollard, *App. Phys. Lett.*, 2013, **102**, 103103.

17. M. D. Doherty, A. Murphy, R. J. Pollard and P. Dawson, *Phys. Rev. X.*, 2013, **3**, 011001.
18. G. A. Wurtz, R. Pollard, W. Hendren, G. P. Wiederrecht, D. J. Gosztola, V. A. Podolskiy and A. V. Zayats, *Nat. Nanotech.,* 2011, **6**, 106-110.
19. P. R. Evans, R. Kullock, W. R. Hendren, R. Atkinson, R. J. Pollard and L. M. Eng, *Adv. Funct. Mater.,* 2008, **18**, 1075-1079.
20. D. P. Lyvers, J. M. Moon, A. V. Kildishev, V. M. Shalaev and A. Wei, *ACS Nano,* 2008, **2**, 2569–2576.
21. M. D. Doherty, A. Murphy, J. McPhillips, R. J. Pollard and P. Dawson, *J. Phys. Chem. C,* 2010, **114**, 19913-19919.
22. A. D. McFarland, M. A. Young, J. A. Dieringer and R. P. Van Duyne, *J. Phys. Chem. B,* 2005, **109**, 11279–11285.
23. E. Fort and S. Gresillon, *J. Phys. D: Appl. Phys.,* 2008, **41**, 013001.
24. Q. Liao, C. Mu, D. Xu, X. Ai, J. Yao and J. Zhang, *Langmuir,* 2009, **25** (8), 4708-4714.
25. S. J. Lee, A. R. Morrill and M. Moskovits, *J. Am. Chem. Soc.,* 2006, **128**, 2200-2201
26. J. Yao, J. Tang, D. Wu, D. Sun, K. Xue, B. Ren, B. Mao and Z. Tian, *Surf. Sci.*, 2002, **514**, 108-116.
27. D. A. Genov, A. K. Sarychev, V. M. Shalaev and A. Wei, *Nano Lett.*, 2004, **4**, 153-158
28. P. Evans, W. R. Hendren, R. Atkinson, G. A. Wurtz, W. Dickson, A.V. Zayats and R.J. Pollard, *Nanotechnology,* 2006, **17** (23), 5746–53.
29. P. B. Johnson and R. W. Christy, *Phys. Rev. B,* 1972, **6**, 4370−4379.
30. E. Le Ru and P. G. Etchegoin, *Principles of Surface-Enhanced Raman Spectroscopy,* Elsevier, Oxford 2009.
31. B. L. Broglin, A. Andreu, N. Dhussa, J. A. Jr. Heath, J. Gerst, B. Dudley, D. Holland and M. El-Kouedi, *Langmuir*, 2007, **23**, 4563-4568.

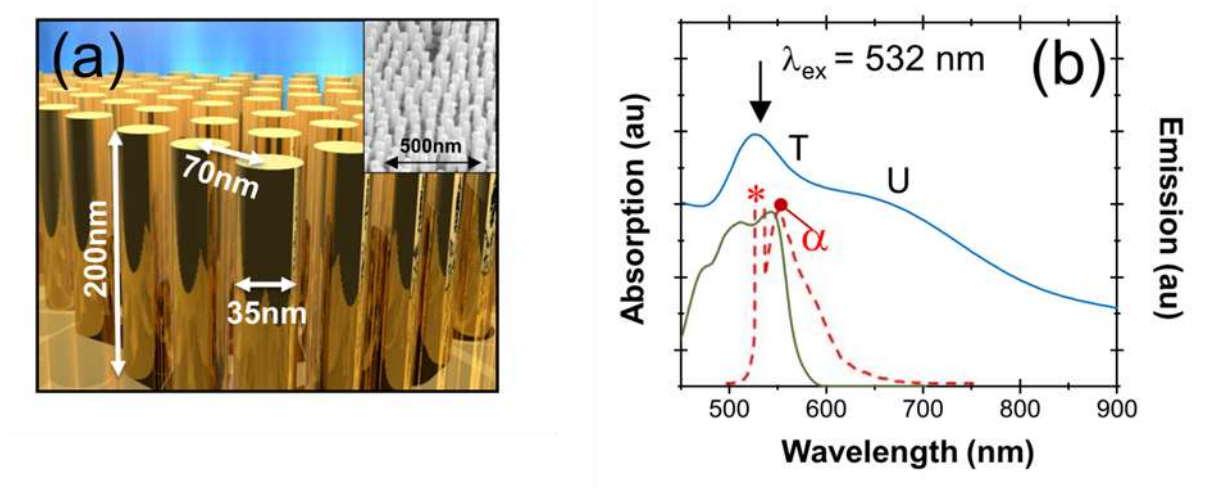

*Fig. 1 a) Schematic drawing of the Au nanorod array, inset shows a SEM image of the array. b) Optical absorption spectrum of the Au nanorod array (blue) and Rhod6G (green). T and U denote the transverse and underlayer plasmonic modes. Emission spectrum of Rhod6G is also shown (red), * denotes peak arising from excitation laser, α = emission max.*

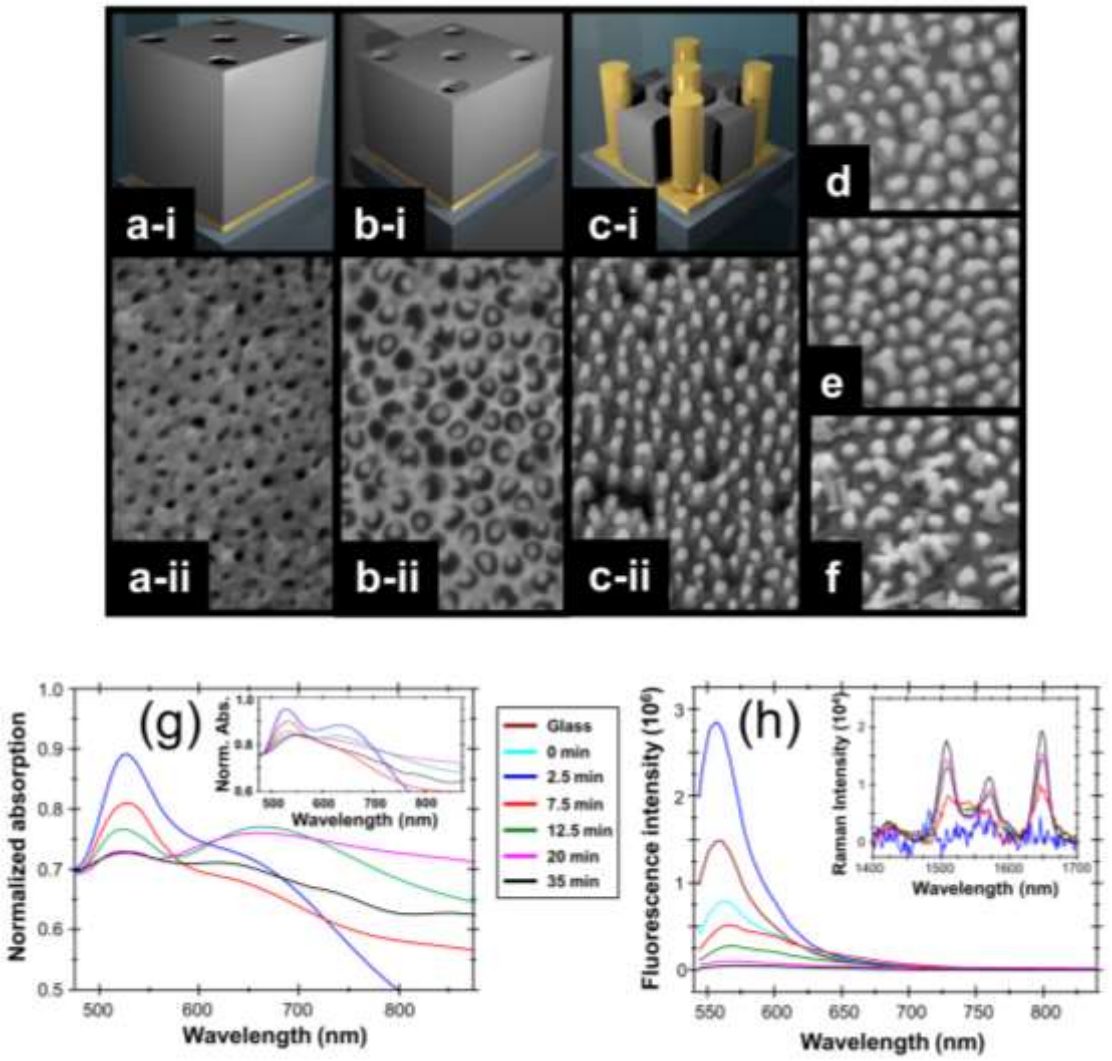

Fig. 2 a-c) Sketches (i) and SEM images (ii) of identical samples etched for three different times, a) 0 min, b) 2.5 min and c) 7.5 min etch. d-f) SEM images of identical samples etched for d) 20 min e) 35 min and f) 40 min. g) Absorption spectra of Au nanorods with Rhod6G, for five different etching times at 0 degrees from normal. Inset shows the absorption spectra recorded from the same samples at 40 degrees from normal. h) Plot of SEF and SERS (inset) signal intensities obtained for different etching times. Fluorescence was also measured from a glass slide, prepared in the same way, as a control.

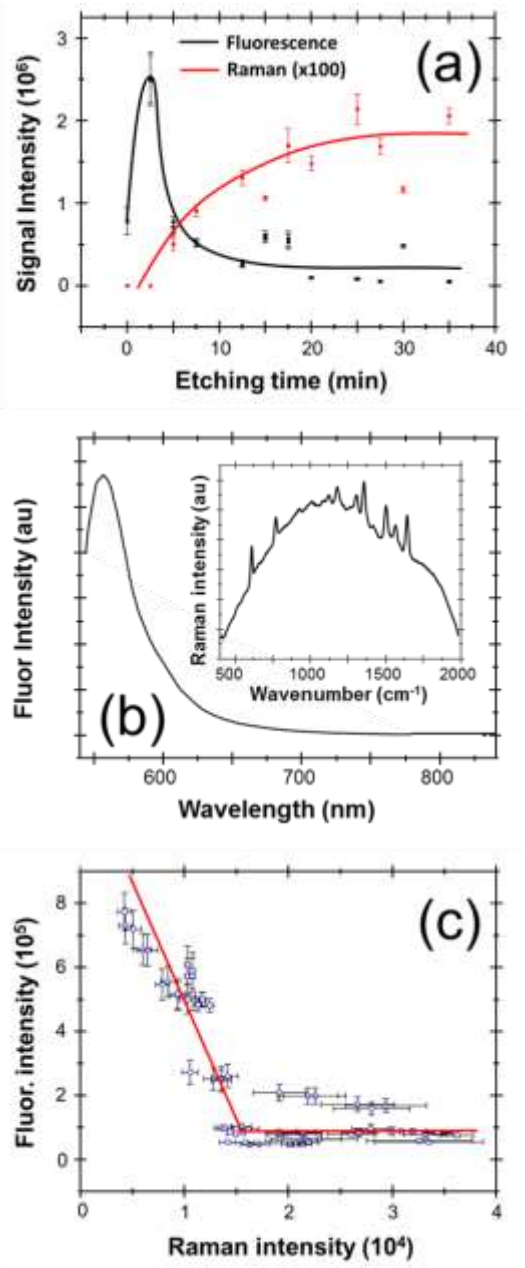

Fig. 3 a) Plot of SEF (■) and SERS (●) signal intensities vs. etching time, noting that SERS intensity has been multiplied by 100. b) Fluorescence spectrum obtained from Rhod6G on Au nanorods, etched for 2.5 min. Inset, Raman spectrum obtained from Rhod6G on the Au nanorods, etched for 35 min. The Raman spectrum is superimposed on the fluorescence peak. c) Plot of SEF vs. SERS intensity (○), obtained simultaneously.

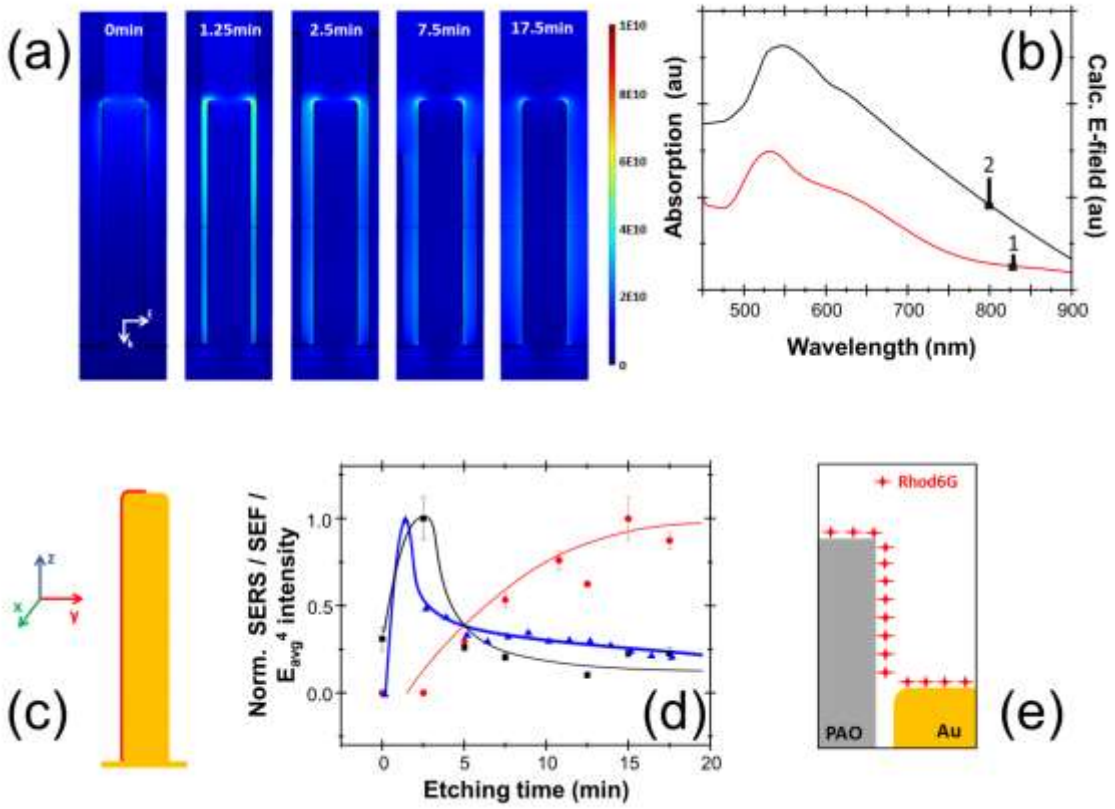

Fig. 4 a) Calculated E-field distribution at excitation wavelength λ=532nm around the Au nanorods for different etching times (0, 1.25, 2.5, 7.5 and 17.5min), with E-field intensity in units of V/m indicated with the color bar. The polarization and wave vector of the incident field are indicated by "E" and "k" respectively. b) Plot of calculated E-field (2) and measured absorption (1) for the structure after 7.5min etching vs. excitation wavelength. c) A model of the Au nanorod is also shown with the area used to calculate the spatial average of the E-field marked with red. d) Plot of measured SEF (■), SERS (●) and calculated E_{avg}^4 (▲) intensities vs. etching time for Au nanorods. e) Diagram showing the position of the probe molecule Rhod6G on the alumina and Au nanorod surface for low etching times.